The Electrochemical Society
Advancing solid state & electrochemical science & technology

Towards an Electrochemical Immunosensor for the Detection of Antibodies against SARS-CoV-2 Spike Protein

View the article online for updates and enhancements.

Towards an Electrochemical Immunosensor for the Detection of Antibodies against SARS-CoV-2 Spike Protein

Viktorija Liustrovaite,[1,=] Maryia Drobysh,[1,2,=] Alma Rucinskiene,[1,2] Ausra Baradoke,[2] Almira Ramanaviciene,[1] Ieva Plikusiene,[1,2] Urte Samukaite-Bubniene,[1] Roman Viter,[3] Chien-Fu Chen,[2] and Arunas Ramanavicius[1,2,z]

[1]NanoTechnas—Center of Nanotechnology and Materials Science, Faculty of Chemistry and Geosciences, Vilnius University, Naugarduko str. 24, 03225 Vilnius, Lithuania
[2]State Research Institute Center for Physical and Technological Sciences, Sauletekio ave. 3, Vilnius, Lithuania
[3]Institute of Atomic Physics and Spectroscopy, University of Latvia, Jelgavas Street 3, Riga, LV-1004, Latvia
[4]Institute of Applied Mechanics, National Taiwan University, 1, Sec. 4, Roosevelt Rd., Da'an Dist., Taipei City 106, Taiwan

Herein we report the electrochemical system for the detection of specific antibodies against severe acute respiratory syndrome coronavirus 2 (SARS-CoV-2) proteins in blood serum patient samples after coronavirus disease 2019 (COVID-19). For this purpose, the recombinant SARS-CoV-2 spike protein (SCoV2-rS) was covalently immobilised on the surface of the gold electrode pre-modified with mixed self-assembled monolayer (SAMmix) consisting of 11-mercaptoundecanoic acid and 6-mercapto-1-hexanol. The affinity interaction of SCoV2-rS with specific antibodies against this protein (anti-rS) was detected using two electrochemical methods: cyclic voltammetry (CV) and electrochemical impedance spectroscopy (EIS). The anti-rS was detected with a detection limit of 2.53 nM and 1.99 nM using CV and EIS methods, respectively. The developed electrochemical immunosensor is suitable for the confirmation of COVID-19 infection or immune response in humans after vaccination.

The severe acute respiratory syndrome coronavirus 2 (SARS-CoV-2) induced coronavirus disease 2019 (COVID-19), is still continuously spreading worldwide. Therefore, the need for rapid and accurate detection methods, including immunosensors, remains relevant to maintain the spread of this infectious disease.[1] The application of immunosensors[2,3] and other affinity sensors[1,4] are of great interest in various clinical diagnostics due to their sensitivity, selectivity, and reliable cost. Antigens, which are recognised by the immune system, and antibodies expressed as the immune system response to the antigen can act as a biorecognition layer or target element in immunosensors suitable for the diagnosis of viral infections.[5,6]

SARS-CoV-2 contains a linear, single-stranded, positive-sense RNA with a length of approximately 29903 nucleotides.[7] The virus has crown-like spikes on the outer surface with a diameter of nearly 130 nm.[8] The genome size is 29.8–29.9 kb and its one-third consists of genes that encode structural proteins including spike (S), envelope (E), membrane (M), and nucleocapsid (N) proteins.[9] The E-protein is the smallest one, and it plays a role in the formation and maturation of the virus. The M-protein can connect with other structural proteins, and its function is to keep the shape of the virus shell.[10] The N-protein is the main structural element of the virion and it participates in viral replication and immune adjustment, it is an inherent attribute in the life cycle of the virus.[11] The S-protein is a homotrimer protein that protrudes from the lipid bilayer surrounding SARS-CoV-2[12,13] and consists of two subunits, namely, S1 and S2. S1 is responsible for binding to the host cell receptor, while S2 mediates viral fusion with the host cell membrane. The S-protein binds to the host cell via the angiotensin-converting enzyme 2 receptors.[14–18]

The S-protein can serve as a biorecognition element of the immunosensor. SARS-CoV-2 infection induces an immune response and the release of specific antibodies,[19] which might be used as a target for immunosensors. Currently, serologic tests for the presence of antibodies against SARS-CoV-2 virus proteins are mainly based on common approaches such as the enzyme-linked immunosorbent assay (ELISA)[20] and the lateral flow immunoassay (LFIA).[21]

Nonetheless, some widely used immunoanalytical methods possess several disadvantages, namely, they are time-consuming (ELISA) and/or not fully automated (LFIA). Therefore, it is necessary to develop rapid, non-laborious, and precise tests with the potential for quantitative analysis. Wherein various physical methods can be used for the determination of analytical signals generated by affinity sensors, including surface plasmon resonance,[22] scanning electrochemical microscopy,[23] electrochemical methods,[24] quartz crystal microbalance,[25] total internal reflection ellipsometry,[26] etc. Among all these analytical methods, electrochemical immunosensors are characterised by some advantages such as low cost, robustness, and simplicity of detection procedure and data interpretation.[24,27]

Only several recent studies are dedicated to the electrochemical technique-based diagnosis of COVID-19.[28–30] Specifically, electrochemical impedance spectroscopy (EIS)[5,31,32] and cyclic voltammetry (CV)[33] are appropriate analytical methods. The EIS is a reliable method for examining the interfacial features of events occurring on transformed surfaces. The small amplitude perturbation from the steady-state is one of the benefits of EIS, which makes it a non-destructive technique.[34] CV is used to acquire data concerning the redox potential and other electrochemical characteristics of analyte solutions. However, CV is also commonly used for observing the processes occurring on the surface of the sensing electrode itself.[35] In particular, this method is a helpful tool to assess blockage of the coated electrode surface.[36]

Immobilisation of the biorecognition element on the conductive surfaces of the electrode is a challenging task during the development of electrochemical affinity sensors.[37] One of the approaches employed for the immobilisation of biomolecules on the surface is the self-assembled monolayer (SAM) technique. Alkanethiol-based monolayers are considered as well-organised and stable interfaces with the necessary thickness and function.[38] Therefore, the application of SAM mixture (SAMmix) consisting of 6-mercapto-1-hexanol (6-MCOH) and 11-mercaptoundecanoic acid (11-MUA) was used to offer an accurate approach for surface modification with desired functional groups and covalent biomolecules immobilisation. Additionally, it minimizes the adsorption of nonspecific proteins on the surface of the working electrode.[39]

The objectives of this study were (i) to explore the possibility to develop an immunosensor for the serologic diagnosis of COVID-19

=These authors contributed equally to this work.
zE-mail: Arunas.Ramanavicius@chf.vu.lt
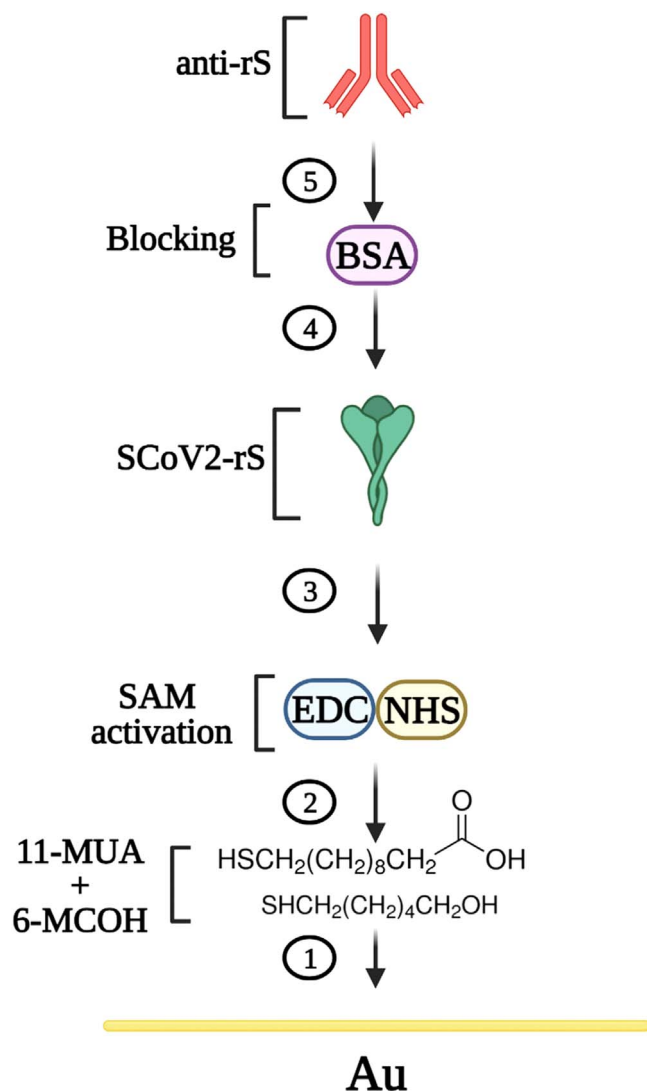
Figure 1. Schematic representation of experimental stages: (1) SAMmix layer formation on Au electrode (Au/SAMmix); (2) SAMmix activation by EDC-NHS mixture (Au/SAMmix/EDC-NHS); (3) SCoV2-rS immobilisation and formation of Au/SAMmix/SCoV2-rS sensing structure; (4) BSA binding of remaining activated carboxyl groups; (5) affinity interaction of anti-rS with immobilised SCoV2-rS (Au/SAMmix/SCoV2-rS/anti-rS).

based on the formation of the recombinant SARS-CoV-2 S-protein (SCoV2-rS) and specific antibodies (anti-rS) immune complex using electrochemical methods; (ii) to improve the measurement conditions and technique for effective immobilisation of SCoV2-rS on the surface of the working electrode for further use in research on other electrochemical methods.

Experimental

Chemicals and other materials.—Microscope slides were obtained from Thermo Fisher Scientific (USA), 2-propanol (2-PrOH), ($\geqslant$99.5%, CAS# 67–63–0), H_2SO_4 (96%, CAS# 7664–93–9), 11-mercaptoundecanoic acid (11-MUA) (98%, CAS# 71310–21–9), 6-mercapto-1-hexanol (6-MCOH) (97%, CAS# 1633–78–9), ethanol (EtOH) (99.9%, CAS# 64–17–5), N-(3-dimethylaminopropyl)-N'-ethyl-carbodiimide hydrochloride (EDC) ($\geqslant$99.0%, CAS# 25952–53–8), bovine serum albumin (BSA) (>98.0%, CAS# 90604–29–8), and phosphate buffered saline (PBS) tablets (pH 7.4) were obtained from Sigma–Aldrich (Steinheim, Germany), N-hydroxysuccinimide (NHS) (98.0%, CAS# 6066–82–6) was purchased from Alfa Aesar

(Karlsruhe, Germany). SARS-CoV-2 recombinant spike protein (SCoV2-rS) was developed by Baltymas (Vilnius, Lithuania). $K_3Fe(CN)_6$ ($\geqslant$99.0%, CAS# 13746–66–2), $K_4Fe(CN)_6$ ($\geqslant$99.0%, CAS# 14459–95–1) were obtained from Sigma–Aldrich (Steinheim, Germany). All aqueous solutions were prepared using deionised water. All chemicals were of analytical-reagent grade and were used as received from the producers unless otherwise stated. All electrochemical measurements were performed in 0.1 M PBS solution adding 2 mM $K_3Fe(CN)_6/K_4Fe(CN)_6$ solution ($[Fe(CN)_6]^{3-/4-}$).

Preparation and/or purification of the SCoV2-rS protein.—The SCoV2-rS protein was generated as a secreted trimeric protein in mammalian Chinese hamster ovary (CHO) cells. To match a native conformation locked in a prefusion state, the gene encoding the SARS-CoV-2 Spike (SCoV2-S) ectodomain including amino acids (aa) 1–1208, (UniProtKB sequence accession number: P0DTC2 (SPIKE_SARS2)) was chemically synthesised at General Biosystems (USA). The synthesised gene then was cloned into the mammalian expression vector pCAGGS (Creative Biogene, cat. no. VET1375) via NotI and XhoI restriction sites that were introduced on 5″ and 3″ gene ends, respectively. The whole expression construct included: full-length SCoV2-S ectodomain (aa 1–1208) w/o transmembrane and cytoplasmic aa, furin cleavage site "RRAR" mutated to "GSAS," C-terminal GSN4 trimerization motif fused to protein sequence, then follows the thrombin cleavage site, Strep-tag II and His6-tag. Two mutations (K986P and V987P) were introduced into the SCoV2-S sequence as well, to stabilize the trimer in the pre-fusion conformation.[18] SCoV2-rS was produced in CHO cells using ExpiCHO Expression System (Thermo Fisher Scientific, cat. no. A29133). For expression, the transfection procedures and expression conditions were applied as described in the Max Titer Protocol provided by Thermo Fisher Scientific. Following the 9th-day post-transfection, the cultivation media was harvested and centrifuged at 5000× g for 30 min in a refrigerated centrifuge. Then the supernatant was filtered through a 0.22 μm filter. After microfiltration, proteins were concentrated and transferred to the binding buffer (50 mM NaH_2PO_4, pH 8.0, 300 mM NaCl, 10 mM imidazole) through tangential ultrafiltration using tangential flow filtration cassette with 100 kDa cut-off membranes (SartoriusStedim Biotech, cat. no. VF20P). The protein solution was loaded onto nickel-nitrilotriacetic acid modified SuperFlow (Qiagen, USA) resin. Non-specifically bound proteins were removed by washing the column with a Lysis buffer containing 75 mM imidazole. Tightly bound proteins were eluted using 75 mM–250 mM imidazole gradient. Fractions containing purified SCoV2-S were pooled and dialysed against PBS (10 mM Na_2HPO_4, 1.8 mM KH_2PO_4, 137 mM NaCl, 2.7 mM KCl, pH 7.4), adjusted to 1.0 mg ml^{-1} concentration, filter-sterilised, aliquoted, and frozen for storage. The purity of produced SCoV2-rS was ~90%, as determined by sodium dodecyl-sulphate polyacrylamide gel electrophoresis.

Serum sample collection.—A volunteer vaccinated with a single dose of the Vaxzevria (previously known as the AstraZeneca) vaccine and who after two weeks had COVID-19 was selected for the analysis. Blood was collected one month after the volunteer was positive, which was determined by reverse transcription-polymerase chain reaction for the SARS-CoV-2 virus and COVID-19 was diagnosed. Whole blood was collected in a vacuette tube containing 3.5 ml of CAT serum sep clot activator (Greiner Bio-One GmbH, Austria) in the laboratory of Tavo Klinika, LtD. (Vilnius, Lithuania). The serum was obtained after centrifugation at 5000× g for 15 min. The stock amount of binding antibodies vs SCoV2-S in the serum sample (4666 BAU ml^{-1}) was defined using chemiluminescent microparticle immunoassay. The antibody concentration in the sample was converted from BAU ml^{-1} units to nM concentration by using the ratio as 1 BAU ml^{-1}: 20 ng ml^{-1} (the molecular weight of immunoglobulin G ~150 kDa).[40–42] Serum sample was stored at −20 °C until analysis. The sample was collected in accordance with
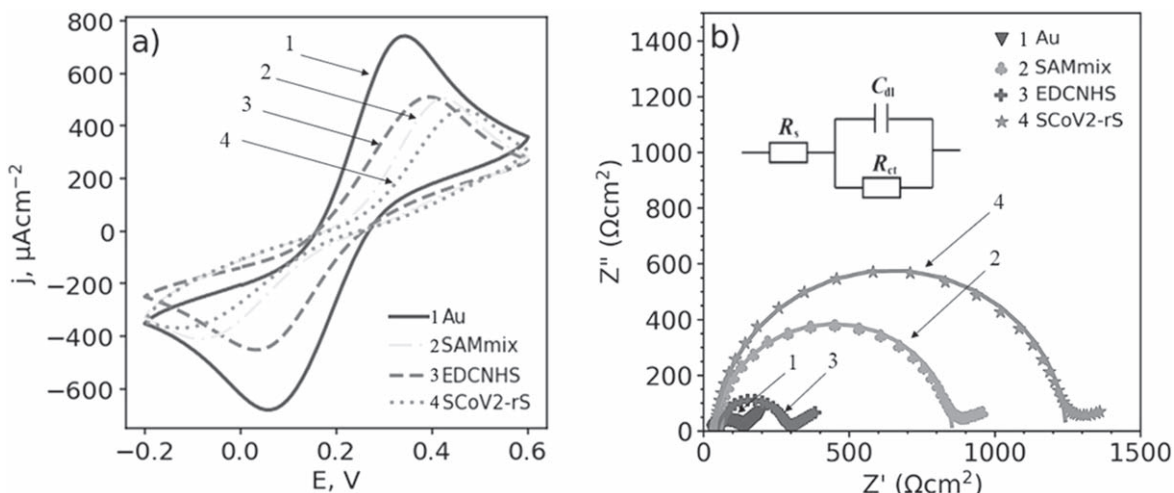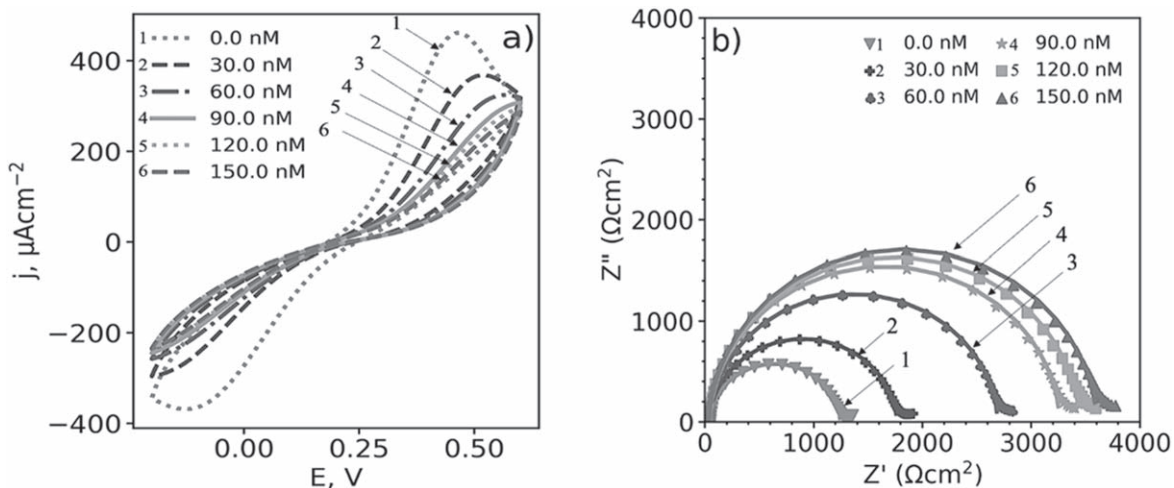
Figure 2. (a)-Cyclic voltammograms of the Au electrode (1), Au/SAMmix electrode after formation of SAMmix (2), Au/SAMmix/EDC-NHS electrode after activation of SAMmix (3), and Au/SAMmix/SCoV2-rS electrode after immobilisation of SCoV2-rS (4). Potential scans range from −0.2 to +0.6 V vs Ag/AgCl(KCl$_{sat}$) at 50 mV s^{-1}. (b) - Nyquist plots of the Au electrode (1), Au/SAMmix electrode after SAMmix formation (2), Au/SAMmix/EDC-NHS electrode after activation of SAMmix (3), and Au/SAMmix/SCoV2-rS electrode after immobilisation of SCoV2-rS (4), measured from 100 kHz to 0.1 Hz, at 10 mV amplitude and applied potential 0.2 V vs Ag/AgCl(KCl$_{sat}$). Randles equivalent circuit, which was applied for the evaluation of electrochemical impedance spectroscopy data, where R_s represents the dynamic solution resistance, C_{dl}—represents the double layer capacitance measured between the Au electrode and the electrolyte solution, and R_{ct}—represents the charge transfer resistance of the immobilised recognition layer. CV and EIS measurements were performed in PBS pH 7.4 while adding 2 mM of [Fe(CN)$_6$]$^{3-/4-}$, signal normalised to the area of the electrode, A = 0.179 cm^2.

the Lithuania ethics law. This study does not need the approval of the ethics committee (confirmed by the Vilnius Regional Biomedical Research Ethics Committee).

Preparation of the gold electrode surface.—Microscope slides 20 × 30 mm were cleaned with 2-PrOH, ultrasonicated (ultrasonic bath Emmi-40 HC, EMAG, Germany) firstly with 2-PrOH, then with water and immersed in H$_2$SO$_4$ for 30 min. The slides were dried with a stream of nitrogen (N$_2$) gas (99.99%) and placed in a vacuum magnetron, VST services Ltd. (Israel), chamber. Film depositions begin only when a vacuum of 7 × 10^{-8} Torr and deeper was reached. The plates were first coated with a thin (10 nm) layer of titanium (Ti) to improve the adhesion of gold (Au) to the surface of the glass and then coated with a (100 nm) layer of Au.

The activation of the SAMmix layer and covalent immobilisation of the SCoV2-rS protein.—The glass slides coated with 100 nm

thick Au film were incubated at 24 °C for 4 h in 1 mM 6-MCOH and 11-MUA ethanolic solution, containing the materials in a molar ratio of 9:1, respectively, to form SAMmix (Fig. 1, step 1). After incubation, the electrode was rinsed with EtOH to remove the excess of SAMmix and then dried with N$_2$ flow. SAMmix formed on the Au electrode (Au/SAMmix) was activated by EDC-NHS mixture. During this procedure, functionally active NHS-esters were obtained by the reaction of 11-MUA carboxyl groups with a mixture of 0.004 M EDC and 0.001 M NHS in PBS (Fig. 1, step 2). The activation step was carried out for 15 min in the dark (Au/SAMmix/EDC-NHS). After activation of carboxyl functional groups, the electrode was exposed to 70 μl of 100 μg ml^{-1} SCoV2-rS in PBS at room temperature for 30 min (Au/SAMmix/EDC-NHS/SCoV2-rS). Protein SCoV2-rS was coupled covalently via primary amine functional groups (Fig. 1, step 3). The remaining reactive esters were deactivated with 0.5% BSA, 30 min (Fig. 1, step 4). Then 100 μl of anti-rS in PBS was added in a concentration range

Figure 3. (a)—Cyclic voltammograms and (b)—Nyquist plots of the modified Au/SAMmix/SCoV2-rS electrode (1) after affinity interaction with anti-rS of different concentrations (0–150 nM) (respectively, from 2 to 6). Potential scans range from −0.2 to +0.6 V vs Ag/AgCl(KCl$_{sat}$) at 50 mV s^{-1}. EIS measurements were performed from 100 kHz to 0.1 Hz, at 10 mV amplitude and applied potential 0.2 V vs Ag/AgCl(KCl$_{sat}$). CV and EIS measurements were performed in PBS pH 7.4, while adding 2 mM of [Fe(CN)$_6$]$^{3-/4-}$, signal normalised to the area of the electrode, A = 0.179 cm^2.

Table I. Analytical parameters were obtained from CV and EIS. Error bars are calculated as a percentage standard error.

	CV	EIS				
Concentration anti-rS, nM	E_{pa}, mV	j_{pa}, $\mu A\ cm^{-2}$	E_{pc}, mV	j_{pc}, $\mu A\ cm^{-2}$	R_{ct}, $\Omega \cdot cm^2$
0	462.6 ± 1.7	460.8 ± 1.6	127.0 ± 0.1	367.9 ± 1.3	1300 ± 105
30	506.6 ± 19.0	382.1 ± 19.3	195.3 ± 6.9	299.8 ± 5.3	1840 ± 165
60	561.5 ± 10.4	329.1 ± 6.6	200.3 ± 0.1	258.7 ± 1.6	2800 ± 212
90	599.4 ± 1.7	310.9 ± 3.5	200.3 ± 0.1	245.7 ± 1.1	3360 ± 286
120	601.1 ± 0.1	296.9 ± 0.6	200.3 ± 0.1	234.6 ± 0.6	3570 ± 259
150	601.1 ± 0.1	287.0 ± 0.8	200.3 ± 0.1	235.7 ± 0.8	3750 ± 319
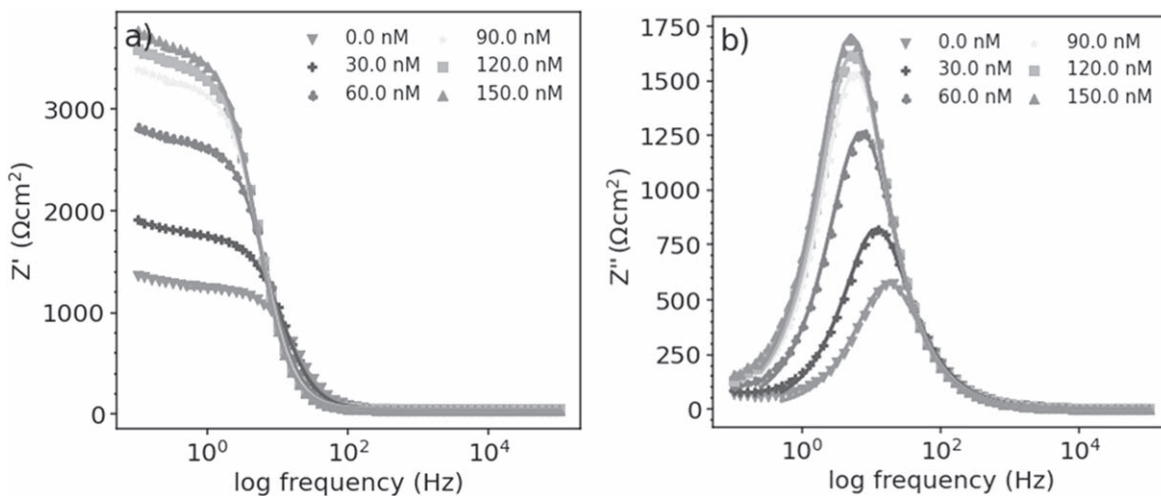
Figure 4. Bode of Z' (a) and Z' (b) vs frequency plots, measured in a range of 0.1 Hz to 100 kHz at a perturbation amplitude of 10 mV and potential 0.2 V vs Ag/AgCl(KCl$_{sat}$). EIS measurements were performed in PBS, pH 7.4, while adding 2 mM of $[Fe(CN)_6]^{3-/4-}$, signal normalised to the area of the electrode, A = 0.179 cm^2.

from 30 to 150 nM and the affinity interaction of specific antibodies with SCoV2-rS immobilised on the electrode was carried out at room temperature for 45 min (Au/SAMmix/EDC-NHS/SCoV2-rS/ anti-rS). After each step of incubation, the structure was rinsed with PBS solution and used further for the electrochemical measurements. The formed Au/SAMmix, Au/SAMmix/EDC-NHS, and Au/ SAMmix/SCoV2-rS electrodes were used in all further electrochemical experiments. The Au/SAMmix/SCoV2-rS electrodes were used for the determination of specific antibodies against the SCoV2-rS protein (Fig. 1, step 5).

Electrochemical measurements.—Electrochemical characterisation of the Au, Au/SAMmix, Au/SAMmix/EDC-NHS, and Au/ SAMmix/SCoV2-rS electrodes was performed using the potentiostat μAUTOLAB TYPE III (Metrohm, Netherland) controlled by FRA2-EIS software from ECO-Chemie (Utrecht, Netherlands). All experiments were performed in the three-electrode electrochemical cell. To bring the experiment closer to in vivo conditions, all experiments prior and after all incubation steps were performed in PBS, pH 7.4 with the addition of 2 mM of $[Fe(CN)_6]^{3-/4-}$ as a redox probe. The three-electrode system consisted of the Au-based electrode (Au, Au/ SAMmix, Au/SAMmix/EDC-NHS, and Au/SAMmix/SCoV2-rS) as the working electrode, platinum (Pt) wire as the counter electrode, and Ag/AgCl in saturated KCl (Ag/AgCl$_{(KClsat)}$) microelectrode (IS-AG/AGCL.AQ.RE) as the reference electrode (ItalSens, The Netherlands). Electrochemical characterisation of bare Au, Au/ SAMmix, Au/SAMmix/EDC-NHS, and Au/SAMmix/SCoV2-rS electrodes at different modification steps were performed using CV and EIS methods. CV measurements were performed in the potential range from −0.2 to +0.6 V vs Ag/AgCl$_{(KClsat)}$, at a scan rate of 50 mV s^{-1}. For the registration of EIS spectra in the frequency range between 0.1 Hz and 100 kHz, a perturbation amplitude of 10 mV and potential 0.2 V vs Ag/AgCl(KCl$_{sat}$) were applied.

Results and Discussion

Electrochemical characterisation of a modified Au surface.— Characterisation of Au, Au/SAMmix, Au/SAMmix/EDC-NHS, and Au/SAMmix/SCoV2-rS electrode has been carried out by CV and EIS methods. The impact of each step of the modification of the working electrode surface on the conductivity has been analysed using a $[Fe(CN)_6]^{3-/4-}$ couple as a redox probe while analysing the oxidation/reduction peaks of the corresponding cyclic voltammogram (Fig. 2a). The 11-MUA forms a stable and compact film, in which the content of pinholes and structural defects in the monolayer is reduced, thereby enabling to observe mediated electron passage kinetics[43]. However, in order to facilitate access of the redox mediator to the electrode surface SAMmix consisting of 6-MCOH and 11-MUA was used[44]. The Au electrode shows a typical cyclic voltammogram (Fig. 2a-1), reversible reaction, characteristic of the redox couple, producing a current density peak of 712.4 ± 5.9 μA cm^{-2}. After modification of the Au electrode with the SAMmix (Fig. 2a-2), the peak decreased to 504.6 ± 19.3 μA cm^{-2}. The EDC-NHS activation (Fig. 2a-3) of the terminal –COOH groups slightly increased the current density to 513.1 ± 6.6 μA cm^{-2}, nevertheless, the immobilisation of SCoV2-rS (Fig. 2a-4) decreased it to 459.6 ± 9.3 μA cm^{-2}.

EIS has been used as an efficient method for the monitoring of impedimetric characteristics and theoretical analysis of impedance properties based on the applied equivalent circuit, enabling the perception of chemical transformation and processes associated with the surface of the conductive electrode[45]. Figure 2b) shows the
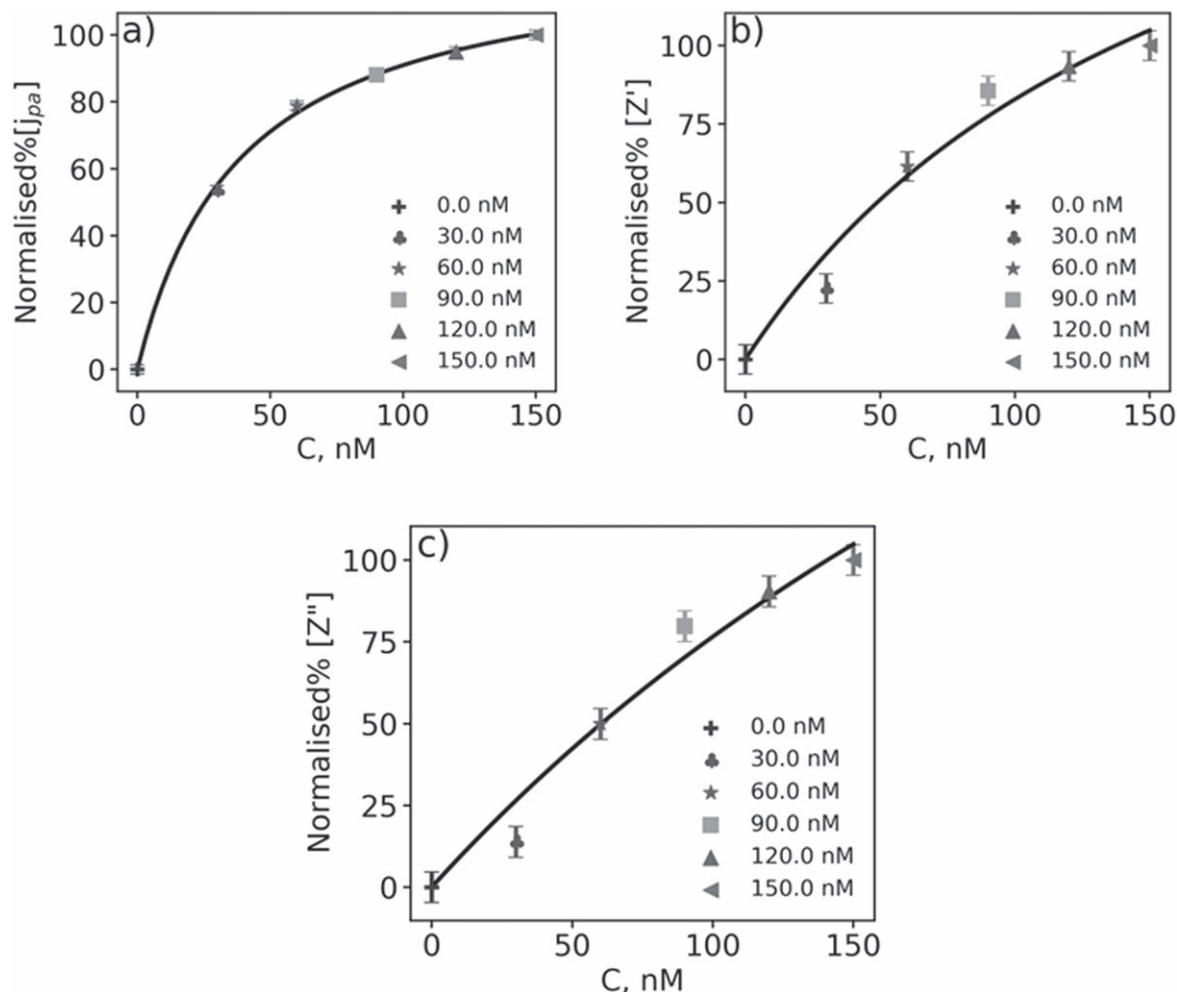
Figure 5. Calibration curves obtained from CV (a) and EIS spectra fitted R_{ct} (b) and EIS maximum of Z″(c). Error bars are calculated as a percentage standard error. Signal normalised to the electrode area, A = 0.179 cm^2.

impedance responses of the $[Fe(CN)_6]^{3-/4-}$ based redox probe in PBS on the Au electrode (Fig. 2b-1), after the formation of the Au/SAMmix structure based on 11-MUA and 6-MCOH, molar ratio 1:9, respectively (Fig. 2b-2), activation of SAMmix with EDC and NHS (Fig. 2b-3), the covalent immobilisation of SCoV2-rS (Fig. 2b-4) in the frequency range from 100 kHz to 0.1 Hz.

The Nyquist coordinates are well suited to represent the electrochemical impedance, especially at the "semi-circular part" of the EIS spectra represented in Fig. 2b). It is shown that after the formation of SAMmix on the Au electrode, the diameter of the semicircle increases. Therefore, when the Au surface was modified, the electron transfer resistance R_{ct} has also increased from 141 ± 34 $\Omega\cdot$cm^2 to 884 ± 163 $\Omega\cdot$cm^2. Then, the activation of the terminal-COOH groups with EDC-NHS forming an intermediate active ester was performed and is led to the decrease of Au/SAMmix/EDC-NHS semicircle as well R_{ct} value down to 300 ± 46 $\Omega\cdot$cm^2.[46] This intermediate product displayed tremendous electrochemical behaviour, the increase in R_{ct} up to 1280 ± 237 $\Omega\cdot$cm^2 after SCoV2-rS binding can be explained by the fact that, at low frequencies, most biological molecules, including proteins, have poor electrical conductivity and therefore impede charge transfer at the interphase between the electrode and solution. For differently modified electrodes, the R_{ct} component tends to have apparent variations, which are providing the high sensitivity required for the detection of antigen-antibody complex formation by the EIS-based technique. Subsequently, after the immobilisation of SCoV2-rS, the deactivation of the remaining

activated carboxyl groups and the blocking of the free surface to avoid non-specific binding are performed using 0.5% solution of BSA.

Electrochemical sensing of anti-rS.—The affinity interaction of anti-rS with immobilised SCoV2-rS was performed by sequentially incubating the working surface with 30 nM of anti-rS PBS solution (the concentration range 30 nM–150 nM). CV and EIS measurements are performed in the presence of 2 mM $[Fe(CN)_6]^{3-/4-}$ in a PBS solution applying the parameters described in the previous part. The concentration range is obtained by successive dilutions of the stock solution.

The affinity interaction of anti-rS with immobilised SCoV2-rS and immune complex formation (Fig. 3a-1) continues to insulate the working electrode surface thereby reducing $Fe[(CN)_6]^{3-/4-}$ flow towards the electrode. Thus, the decrease in redox current is the stepwise flattening of the cyclic voltammograms with increasing anti-rS concentration (Fig. 3a). Partial coating of the electrode surface with the increasing concentrations of anti-rS causes a corresponding decrease of anodic (j_{pa}) and cathodic (j_{pc}) current density at the range of potentials from 460 mV to 600 mV and from −130 mV to −200 mV, respectively (Table I). The potential shift with increasing concentration of anti-rS can be explained due to hindered electron exchange at the Au electrode surface as a result of biomolecules binding, thereby, affecting the value of the redox reaction potential. Noteworthy, that for lower concentrations
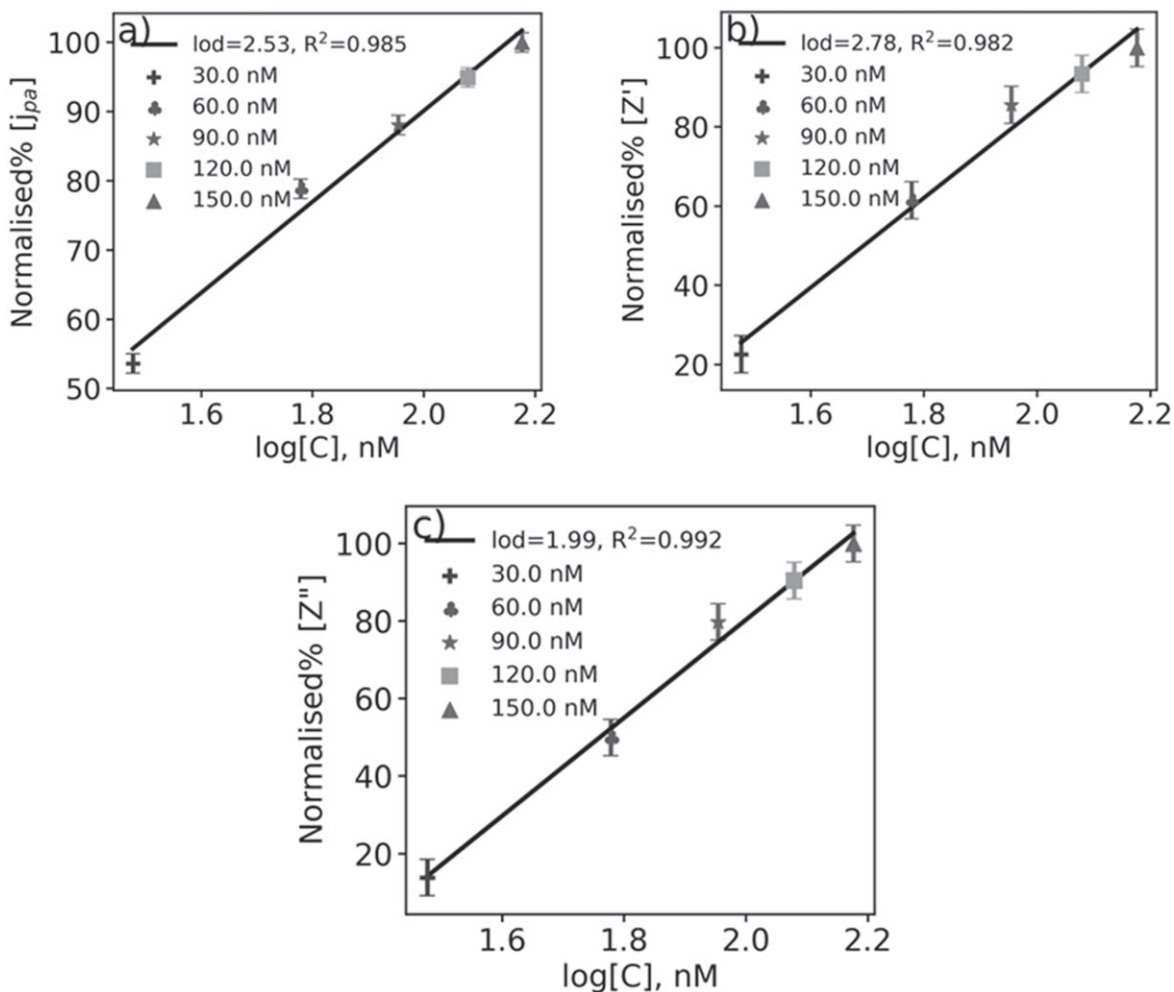
Figure 6. Calibration curves obtained from CV (a) and EIS fitted R_{ct} (b), EIS, maximum of Z″ (c). Error bars are calculated as a percentage standard error. Signal normalised to electrode area, A = 0.179 cm^2.

(0−90 nM) of anti-rS, the values of maximum current densities decrease faster, while for higher concentrations (90 − 150 nM) the process reaches saturation point (Figs. 4 and 5).

The same effect is accompanied by a sequential growth of the semicircle radius in the Nyquist plot (Fig. 3b). EIS reveals the broad trend for radii growth toward lower concentrations (0 − 90 nM) and a slowdown in the radii growth at high concentrations (90–150 nM). The number of non-occupied SCoV2-rS decrease with the increase of antibody concentration and obtained signal values from CV and EIS are summarised in Table I, where the dependence of the increased R_{ct} value vs concentration tends to plateau at high content of anti-rS.

Analytical characterisation of the immunosensor developed for the anti-rS detection.—To evaluate the analytical characteristics of the electrochemical immunosensor, limits of detection (LODs) for sensing anti-rS were calculated from CV and EIS measurements. From CV, the highest value of the anodic current density (j_{pa}) and the lowest value of cathodic current density (j_{pc}) was used as the signal. From EIS, as a signal, the R_{ct} value (obtained as a maximum value of Z′) and maximum of Z″ were used.

The values of data in Table I, were normalised using the equation:

$$zi = (xi - \min(x))/(\max(x) - \min(x)) \times 100,$$

where zi - the value of *Normalised%*, xi - extracted electrochemical parameter (j_{pa}, Z′$_{max}$, Z″$_{max}$) at each concentration of anti-rS; min(x)

—the minimum value in the list of each extracted electrochemical parameter; max(x)—the maximum value of each extracted electrochemical parameter. Obtained values of the normalised signal (*Normalised%*) vs the concentration of anti-rS were plotted and shown in the Figs. 5 and 6.

The Langmuir fit was obtained by fitting the Normalised signal (as *y*-value) and concentration data (as *x*-value) to equation:

$$y = B_{\max} \times x/(K_d + x),$$

where $B_{\max}$—maximum value obtained during specific binding and K_d- equilibrium dissociation constant, a concentration needed to achieve a half-maximum binding at equilibrium. K_d values of 37 nM and 39 nM were obtained from parameters extracted in CV data. Similar values (19–33 nM) were reported in a previous work, where C-reactive protein was investigated.[47]

The equation:

$$LOD = 3\sigma/slope,$$

where σ is the standard deviation of the y-intercept of the standard plot ((Normalised%) vs target concentration) was used for LODs calculation.[48] As a result, immunosensor for anti-rS detection by the CV using j_{pa}, is characterised by LOD of 2.53 nM and it was defined from the standard plot shown in Fig. 6a. For comparison, the LOD obtained from CV in the cathodic area was twice higher, giving the value of 5.85 nM, which could be explained by slower electron charge transfer in the cathodic region. LODs for EIS based method (Figs. 6b

and 6c) were calculated and compared for several methodologies of data analysis. When a plot of *Normalised%* calculated using the R_{ct} value vs concentration was used, the LOD with a value of 2.78 nM was obtained. For comparison, the LOD value obtained from the maximum of the Z'' peak was 1.99 nM, which is 38% lower.

Conclusions

In this study, the covalent immobilisation of SCoV2-rS and its affinity interaction with anti-rS were evaluated. The surface of the Au electrode was characterised by CV and EIS methods after each modification step. CVs revealed that the peak current density measured with the addition of 2 mM $[Fe(CN)_6]^{3-/4-}$ decreased after the formation of the SAMmix on the electrode surface. EIS spectra represented in Nyquist coordinates indicate evident changes in every step of Au electrode modification. The charge transfer resistance of the Au/SAMmix electrode after activation with EDC and NHS decreased compared to the electrode before activation, while the semicircle increases after immobilisation of SCoV2-rS and affinity interaction with anti-rS. The anti-rS antibodies were quantified using CV and EIS methods, giving the lowest LOD values of 2.53 nM and 1.99 nM, respectively. This allows the application of impedimetric methods to detect the formation of antigen-antibody complexes and the subsequent development of an immunosensor for the serologic diagnosis of COVID-19 and/or the determination of the success of vaccination against the SARS-CoV-2 virus.

Acknowledgments

ORCID

Arunas Ramanavicius ⬤ https://orcid.org/0000-0002-0885-3556

References

1. M. Drobysh, A. Ramanaviciene, R. Viter, and A. Ramanavicius, *Micromachines*, **12**, 390 (2021).
2. S. Ramanavicius and A. Ramanavicius, *Polymers (Basel).*, **13**, 1 (2021).
3. S. Ramanavicius and A. Ramanavicius, *Int. J. Mol. Sci.*, **21**, 1 (2020).
4. S. Ramanavicius, A. Jagminas, and A. Ramanavicius, *Polymers (Basel).*, **13**, 1150 (2021).
5. A. Ramanavicius, A. Finkelsteinas, H. Cesiulis, and A. Ramanaviciene, *Bioelectrochemistry*, **79**, 11 (2010).
6. I. Plikusiene, V. Maciulis, A. Ramanaviciene, Z. Balevicius, E. Buzavaite-Verteliene, E. Ciplys, R. Slibinskas, M. Simanavicius, A. Zvirbliene, and A. Ramanavicius, *J. Colloid Interface Sci.*, **594**, 195 (2021).
7. F. Wu et al., *Nature*, **579**, 265 (2020).
8. M. Laue, A. Kauter, T. Hoffmann, J. Michel, and A. Nitsche, *Sci Rep*, **11**, 3515 (2021).
9. R. A. Khailany, M. Safdar, and M. Ozaslan, *Gene Reports*, **19**, 100682 (2020).
10. I. Astuti and Ysrafil, *Diabetes Metab. Syndr. Clin. Res. Rev.*, **14**, 407 (2020).
11. Y. Peng, N. Du, Y. Lei, S. Dorje, J. Qi, T. Luo, G. F. Gao, and H. Song, *EMBO J.*, **39** (2020).
12. B. W. Neuman et al., *J. Struct. Biol.*, **174**, 11 (2011).
13. M. Bárcena, G. T. Oostergetel, W. Bartelink, F. G. A. Faas, A. Verkleij, P. J. M. Rottier, A. J. Koster, and B. J. Bosch, *Proc. Natl Acad. Sci. USA*, **106**, 582 (2009).
14. A. C. Walls, Y. J. Park, M. A. Tortorici, A. Wall, A. T. McGuire, and D. Veesler, *Cell*, **181**, 281 (2020).
15. M. Hoffmann et al., *Cell*, **181**, 271 (2020).
16. J. Shang, G. Ye, K. Shi, Y. Wan, C. Luo, H. Aihara, Q. Geng, A. Auerbach, and F. Li, *Nature*, **581**, 221 (2020).
17. Q. Wang et al., *Cell*, **181**, 894 (2020).
18. D. Wrapp, N. Wang, K. S. Corbett, J. A. Goldsmith, C. L. Hsieh, O. Abiona, B. S. Graham, and J. S. McLellan, *Science (80-.).*, **367**, 1260 (2020).
19. N. Post et al., *PLoS One*, **15**, e0244126 (2020).
20. A. E. Dhamad and M. A. A. Rhida, *PeerJ*, **8**, e10180 (2020).
21. Z. Li et al., *J. Med. Virol.*, **92**, 1518 (2020).
22. A. Kausaite-Minkstimiene, A. Ramanavicius, J. Ruksnaite, and A. Ramanaviciene, *Anal. Methods*, **5**, 4757 (2013).
23. I. Morkvenaite-Vilkonciene, A. Ramanaviciene, A. Kisieliute, V. Bucinskas, and A. Ramanavicius, *Biosens. Bioelectron.*, **141**, 111411 (2019).
24. A. Ramanaviciene and A. Ramanavicius, *Anal. Bioanal. Chem.*, **379**, 287 (2004).
25. D. Plausinaitis, L. Sinkevicius, U. Samukaite-Bubniene, V. Ratautaite, and A. Ramanavicius, *Talanta*, **220** (2020).
26. Z. Balevicius, A. Ramanaviciene, I. Baleviciute, A. Makaraviciute, L. Mikoliunaite, and A. Ramanavicius, *Sensors Actuators, B Chem.*, **160**, 555 (2011).
27. F. Cui and H. S. Zhou, *Biosens. Bioelectron.*, **165**, 112349 (2020).
28. A. Raziq, A. Kidakova, R. Boroznjak, J. Reut, A. Öpik, and V. Syritski, *Biosens. Bioelectron.*, **178**113029 (2021).
29. H. Zhao et al., *Sensors Actuators B Chem.*, **327**, 128899 (2021).
30. Z. S. Miripour et al., *Biosens. Bioelectron.*, **165**, 112435 (2020).
31. A. Baradoke, B. Jose, R. Pauliukaite, and R. J. Forster, *Electrochim. Acta*, **306**, 299 (2019).
32. A. Baradoke, A. Santos, P. R. Bueno, and J. J. Davis, *Biosens. Bioelectron.*, **172**, 112705 (2021).
33. M. H. F. Taha, H. Ashraf, and W. Caesarendra, *Appl. Syst. Innov.*, **3**, 1 (2020).
34. E. B. Bahadir and M. K. Sezgintürk, *Artif. Cells, Nanomedicine Biotechnol.*, **44**, 248 (2016).
35. D. Grieshaber, R. MacKenzie, J. Vörös, and E. Reimhult, *Sensors*, **8**, 1400 (2008).
36. V. Ganesh, S. K. Pal, S. Kumar, and V. Lakshminarayanan, *J. Colloid Interface Sci.*, **296**, 195 (2006).
37. A. Ramanaviciene and A. Ramanavicius, *Crit. Rev. Anal. Chem.*, **32**, 245 (2002).
38. H. G. Hong, W. Park, and E. Yu, *J. Electroanal. Chem.*, **476**, 177 (1999).
39. A. Kausaite-Minkstimiene, A. Ramanaviciene, J. Kirlyte, and A. Ramanavicius, *Anal. Chem.*, **82**, 6401 (2010).
40. National Institute for Biological Standards and Control, 20/136WHO International Standard (2020), https://www.nibsc.org/documents/ifu/20-136.pdf.
41. Immundiagnostik AG, (2021), Manual, https://www.immundiagnostik.com/media/pages/testkits/k-5004/e859ef5a82-1647482477/k5004_2021-08-10_idk_sars-cov-2-igg.pdf.
42. D. J. Dietzen, *Principles and Applications of Molecular Diagnostics*, ed. N. Rifai and A. R. Horvath (Elsevier, Amsterdam) p. 345 (2018).
43. F. Cecchet, M. Marcaccio, M. Margotti, F. Paolucci, S. Rapino, and P. Rudolf, *J. Phys. Chem. B*, **110**, 2241 (2006).
44. V. Rajesh, V. K. Sharma, S. K. Tanwar, Mishra, and A. M. Biradar, *Thin Solid Films*, **519**, 1167 (2010).
45. F. Patolsky, B. Filanovsky, E. Katz, and I. Willner, *J. Phys. Chem. B*, **102**, 10359 (1998).
46. E. B. Bahadir and M. K. Sezgintürk, *Artif. Cells, Nanomedicine Biotechnol.*, **44**, 462 (2016).
47. A. Baradoke, R. Hein, X. Li, and J. J. Davis, *Anal. Chem.*, **92**, 3508 (2020).
48. A. Shrivastava and V. Gupta, *Chronicles Young Sci.*, **2**, 21 (2011).